Grid-based methods for diatomic quantum scattering problems II: Time-dependent treatment of single- and two-photon ionization of H_2^+

Liang Tao,[1] C. W. McCurdy,[1,2] and T. N. Rescigno[1]

[1]*Lawrence Berkeley National Laboratory, Chemical Sciences, Berkeley, CA 94720*
[2]*Departments of Applied Science and Chemistry, University of California, Davis, CA 95616*

(Dated: June 2, 2009)

The time-dependent Schrödinger equation for H_2^+ in a time-varying electromagnetic field is solved in the fixed-nuclei approximation using a previously developed finite-element/ discrete variable representation in prolate spheroidal coordinates. Amplitudes for single- and two-photon ionization are obtained using the method of exterior complex scaling to effectively propagate the field-free solutions from the end of the radiation pulse to infinite times. Cross sections are presented for one-and two-photon ionization for both parallel and perpendicular polarization of the photon field, as well as photoelectron angular distributions for two-photon ionization.

PACS numbers: 33.80.-b, 33.80.Rv,32-80.-.t, 31.15.-p

I. INTRODUCTION

The development of increasingly powerful short-wavelength high-harmonic and free-electron laser sources has intensified the study of multi-photon ionization processes in atoms and molecules. These studies have also provided an impetus for the continued development and refinement of advanced, grid-based nonperturbative methods for numerical solution of the Schrödinger equation. In an earlier paper [1], hereafter referred to as I, showed how to combine finite elements and the discrete variable representation in prolate spheroidal coordinates to develop a grid-based approach for quantum mechanical studies involving diatomic molecular targets. The methodology was illustrated with solutions of the time-independent Schrödinger equation for the bound and continuum states of H_2^+. Here, the finite-element/discrete variable representation in prolate spheroidal coordinates is used in connection with exterior complex scaling to study H_2^+ in a time-varying electromagnetic field.

Our treatment is based on a procedure we introduced to study atomic ionization by short laser pulses. We first solve the time-dependent Schrödinger equation on a real grid for a finite time interval when the target is interacting with a laser pulse. At the termination of the pulse, the wavepacket continues to evolve with the field-free target Hamiltonian, so the propagation to infinite times can be carried out by using the wavepacket at the end of the pulse as a source term in a time-independent driven Schrödinger equation. Exterior Complex Scaling (ECS) is used to enforce proper outgoing wave boundary conditions. From a single wavepacket, we can then construct amplitudes for ejecting electrons in arbitrary directions at any energy within the bandwidth of the pulse. From these amplitudes we can unambiguously construct the cross sections (in the case of one-photon ionization) or generalized cross sections for multiphoton ionization.

Our purpose in this work is to test the efficiency and reliability of the implementation of these ideas with prolate spheroidal coordinates in time-dependent applications on a linear molecule. We will demonstrate that the combination of the three components of this approach, prolate spheroidal coordinates, the DVR representation of the Hamiltonian, and ECS for extracting amplitudes, provides a powerful new algorithm for more general application to diatomic molecules.

The calculations are carried out in the fixed-nuclei (Born-Oppenheimer) approximation, but we present results for both parallel and perpendicular photon polarizations. These amplitudes can then be used to extract molecular-frame ionization probabilities for arbitrary photon polarizations. We will also present body-frame photoelectron angular distributions for two-photon ionization. Although the calculations can be carried out with arbitrary field strengths, we confine our attention here to relatively low intensity fields so that we can compare with the results of other studies that use time-independent methods to calculate cross sections in the perturbative limit. We use atomic units (a.u.) unless otherwise specified.

II. THEORY AND COMPUTATION

A. Solving time-dependent Schrödinger equation in prolate spheroidal coordinates

Our procedure for designing a grid-based set of functions combining the discrete variable representation (DVR) with finite-elements (FEM) in prolate spheroidal coordinates, as well as details about the computation of H_2^+ continuum wavfunctions using exterior complex scaling (ECS) , has been given in I [1] and will not be repeated here. We begin with an expression for the Hamiltonian for H_2^+, including a time-varying electromagnetic field in the velocity gauge:

$$\begin{aligned} H(t) &= -\frac{1}{2}\nabla^2 + \mathcal{V} - i\frac{\mathbf{A}(t)}{c}\cdot\boldsymbol{\nabla} \\ &\equiv H_0 - i\frac{\mathbf{A}(t)}{c}\cdot\boldsymbol{\nabla}\,, \end{aligned} \tag{1}$$

where $\mathcal{V}$ is Coulomb interaction between the electron and the (fixed) nuclei, $\mathbf{A}(t)$ is the vector potential and c is the speed of light. Prolate spheroidal coordinates (ξ, η, ϕ) are defined by rotating a two-dimensional elliptic coordinate system about the focal axis of the ellipse. The angle of rotation is defined by ϕ $(0 \le \phi \le 2\pi)$. With the foci located at $\pm a$ along the $z-$axis and r_1 and r_2 denoting the distances to the two foci, the dimensionless coordinates (ξ, η) are defined as

$$\begin{aligned} \xi &= \frac{r_1 + r_2}{R} \quad (1 \le \xi \le \infty) \\ \eta &= \frac{r_1 - r_2}{R} \quad (-1 \le \eta \le 1)\,, \end{aligned} \tag{2}$$

where $R = 2a$. The Laplacian in these coordinates is

$$\nabla^2 = \frac{4}{R^2(\xi^2-\eta^2)} \left[\begin{array}{l} \frac{\partial}{\partial\xi}(\xi^2-1)\frac{\partial}{\partial\xi} + \frac{\partial}{\partial\eta}(1-\eta^2)\frac{\partial}{\partial\eta} \\ + \left(\frac{1}{(\xi^2-1)} + \frac{1}{(1-\eta^2)}\right)\frac{\partial^2}{\partial\phi^2} \end{array} \right], \tag{3}$$

while the Coulomb interaction is

$$\mathcal{V}(\xi,\eta) = -\frac{1}{r_1} - \frac{1}{r_2} = -\frac{4\xi}{R(\xi^2-\eta^2)}\,. \tag{4}$$

The gradient operator $\boldsymbol{\nabla} = (\partial/\partial x, \partial/\partial y, \partial/\partial z)$ is given by

$$\begin{aligned} \frac{\partial}{\partial x} &= \frac{2\sqrt{(\xi^2-1)(1-\eta^2)}\cos\phi}{R(\xi^2-\eta^2)}\left[\xi\frac{\partial}{\partial\xi} - \eta\frac{\partial}{\partial\eta}\right] \\ &\quad - \frac{2\sin\phi}{R\sqrt{(\xi^2-1)(1-\eta^2)}}\frac{\partial}{\partial\phi} \\ \frac{\partial}{\partial y} &= \frac{2\sqrt{(\xi^2-1)(1-\eta^2)}\sin\phi}{R(\xi^2-\eta^2)}\left[\xi\frac{\partial}{\partial\xi} - \eta\frac{\partial}{\partial\eta}\right] \\ &\quad + \frac{2\cos\phi}{R\sqrt{(\xi^2-1)(1-\eta^2)}}\frac{\partial}{\partial\phi} \\ \frac{\partial}{\partial z} &= \frac{2}{R(\xi^2-\eta^2)}\left[\eta(\xi^2-1)\frac{\partial}{\partial\xi} + \xi(1-\eta^2)\frac{\partial}{\partial\eta}\right] \end{aligned} \tag{5}$$

and the vector potential $\mathbf{A}(t)$ is represented, in the dipole approximation, using a sine squared pulse with photon energy ω and total pulse duration T

$$\mathbf{A}(t) = \begin{cases} A_0 \sin^2\left(\frac{\pi}{T}t\right)\sin(\omega t)\boldsymbol{\epsilon}, & t \in [0,T] \\ 0, & t > T \end{cases} \tag{6}$$

where $\boldsymbol{\epsilon}$ is the linear polarization vector defined by its three components in Cartesian coordinates $(\epsilon_x, \epsilon_y, \epsilon_z)$, and the number of cycles in the pulse duration T is $T\omega/2\pi$.

Our objective here is to solve the time-dependent Schrödinger equation. To that end, we employ the close-coupling DVR scheme outlined in paper I, expanding the time-dependent electronic wave function in a product basis of DVR functions $\chi_i^{lm}(\xi)$ and spherical harmonics Y_{lm} in the variables (η, ϕ):

$$\Psi(\mathbf{r},t) = \sum_i \sum_{l,m} c_i(t)\chi_i^{l,m}(\xi)Y_{l,m}(\eta,\phi). \tag{7}$$

Since the volume element in this coordinate system is $dV = (R/2)^3(\xi^2-\eta^2)d\xi d\eta d\phi$, the basis functions are not orthogonal [1].

We use an implicit Crank-Nicolson propagator to carry out the time integration, where the overlap matrix has to be carried during the propagation. Taking the advantage of the Krylov iterative linear solver from the PETSc library [2], this propagator is easily implemented on massively parallel computers, making it possible to propagate the wave packet under the effect of a long pulse including many cycles. Given the expansion of Eq. (7), we write the time-dependent Schrödinger equation in matrix form:

$$i\mathbf{S}\frac{d}{dt}\mathbf{c}(t) = \mathbf{H}(t)\mathbf{c}(t) \tag{8}$$

where $\mathbf{S}$ and $\mathbf{H}(t)$ are the overlap and Hamiltonian matrices defined with the volume element dV.

An approximate solution of Eq. (8) is

$$\mathbf{c}(t+\Delta t) = e^{-i\mathbf{S}^{-1}\mathbf{H}(t+\frac{1}{2}\Delta t)}\mathbf{c}(t). \tag{9}$$

It follows that the norm of the wavepacket is conserved during the time evolution,

$$\mathbf{c}^+(t)\mathbf{S}\mathbf{c}(t) = 1 \tag{10}$$

The Crank-Nicolson propagator approximates Eq. (9) as

$$\begin{aligned} \mathbf{c}(t+\Delta t) &= \left(1 + \frac{1}{2}i\mathbf{S}^{-1}\mathbf{H}(t+\frac{1}{2}\Delta t)\Delta t\right)^{-1}\left(1 - \frac{1}{2}i\mathbf{S}^{-1}\mathbf{H}(t+\frac{1}{2}\Delta t)\Delta t\right)\mathbf{c}(t) \\ &= \left(\mathbf{S} + \frac{1}{2}i\mathbf{H}(t+\frac{1}{2}\Delta t)\Delta t\right)^{-1}\left(\mathbf{S} - \frac{1}{2}i\mathbf{H}(t+\frac{1}{2}\Delta t)\Delta t\right)\mathbf{c}(t) \end{aligned} \tag{11}$$

This implicit algorithm requires the solution of a linear system at every time step and generally requires a pre-

conditioner for convergence. However, the Hamiltonian doesn't change very much under the effect of a time-dependent perturbation between successive time steps. We have found that we could use the same preconditioner matrix for the entire time propagation, updating only the linear system at each time step and using the solution from the previous time step as the initial guess for the next solve when using Krylov iterative linear solvers. This method enables us to efficiently propagate Eq. (11) on a large grid using parallel computers.

B. Photoionization amplitude construction

The propagated wave packet at the end of the pulse is used as the source term in an after-pulse, driven equation $(E_k - H_0)\Psi_{\rm sc}(\mathbf{r}) = \Psi(\mathbf{r}, T)$, which effectively propagates the wave packet to $T \to \infty$. This equation is solved under ECS to enforce pure outgoing wave boundary conditions. Photoionization amplitudes at different ejected electron energies E_k are then extracted from $\Psi_{\rm sc}(\mathbf{r})$ as outlined in refs. [3, 4]. The only difference is that here we are using a non-orthogonal basis in prolate spheroidal coordinates and therefore the overlap matrix has to be carried when solving the driven equation, written in matrix form as

$$(E_k \cdot \mathbf{S} - \mathbf{H_0})\mathbf{c}_{sc} = \mathbf{S} \cdot \mathbf{c}(T)\,. \tag{12}$$

Having solved Eq. (12) for the scattered wave function $\Psi_{\rm sc}$, the amplitude $C(\mathbf{r})$ for photoionization is constructed in the form of a surface integral

$$C(\mathbf{k}) = \langle \Phi^{(-)}(\mathbf{k},\mathbf{r})\,|E_k - H_0|\,\Psi_{\rm sc}(\mathbf{r})\rangle = \frac{1}{2}\iint \left[\Phi^{(-)*}(\mathbf{k},\mathbf{r})\nabla\Psi_{\rm sc}(\mathbf{r}) - \Psi_{\rm sc}(\mathbf{r})\nabla\Phi^{(-)*}(\mathbf{k},\mathbf{r})\right]\cdot d\mathbf{S}\,, \tag{13}$$

where $\Phi^{(-)}(\mathbf{k},\mathbf{r})$ is a continuum state of H_2^+ with outgoing momentum $\mathbf{k}$, whose calculation in prolate spheroidal coordinatres is detailed in I. Writing the expansion of $\Psi_{\rm sc}(\mathbf{r})$ as

$$\begin{aligned}\Psi_{sc}(\mathbf{r}) &= \sum_{i,l,m} a_i^{lm}\chi_i^{lm}(\xi)Y_{l,m}(\eta,\phi) \\ &\equiv \sum_{l,m}\Lambda_{l.m}(\xi)Y_{l,m}(\eta,\phi)\,,\end{aligned} \tag{14}$$

and similarly for $\Phi^{(-)}(\mathbf{k},\mathbf{r})$ (see Eqs. (24), (26) and (30) of paper I)

$$\begin{aligned}\Phi^{(-)}(\mathbf{k},\mathbf{r}) &= \left(\frac{2}{\pi}\right)^{1/2}\sum_{l_0,m} i^{l_0}e^{i\eta_{l_0}(k)}Y^*_{l_0,m}(\hat{\mathbf{k}}(\theta,\phi)) \\ &\quad\times\sum_{i,l} b_i^{lm}\chi_i^{lm}(\xi)Y_{l,m}(\eta,\phi) \\ &\equiv \left(\frac{2}{\pi}\right)^{1/2}\sum_{l_0,m} i^{l_0}e^{i\eta_{l_0}(k)}Y^*_{l_0,m}(\hat{\mathbf{k}}(\theta,\phi)) \\ &\quad\times\sum_{l}\Omega_l^{l_0,m}(\xi)Y_{l,m}(\eta,\phi)\,,\end{aligned} \tag{15}$$

the photoionization amplitude $C(\mathbf{k})$ is explicitly evaluated as

$$C(\mathbf{k}) = \sum_{l_0,m} i^{-l_0}e^{i\eta_{l_0}(k)}c_{l_0,m}(k)Y_{l_0,m}(\hat{\mathbf{k}}(\theta,\phi)) \tag{16}$$

where

$$\begin{aligned}c_{l_0,m}(k) =& \frac{R}{4}\left(\frac{2}{\pi}\right)^{1/2} \\ &\times\sum_l W\left\{\Lambda_{l,m}(\xi),\Omega_l^{l_0,m}(\xi)\right\}\left(\xi^2-1\right)\Big|_{\xi=\xi_0}\,.\end{aligned} \tag{17}$$

Here the notation $W\{a,b\} \equiv a'b - b'a$ denotes the Wronskian with respect to ξ. In our numerical evaluation of Eq. (17), we generally fix ξ_0 at a real value slightly less than the complex ECS turning point.

In order to distinguish between contributions to one and two-photon ionization, with the molecule oriented either parallel or perpendicular to the polarization axis of the laser field, the quantum numbers m and l in Eq. (16) are appropriately restricted. In Table I, we list all the cases which relate to the results presented in this paper.

The use of exact H_2^+ continuum states in the surface integral expression for $C(\mathbf{k})$ provides complete dynamical information about photoelectron ejection, within the bandwidth of the pulse used during the time propagation, and also removes any contaminating contributions from bound-state excitation because of orthogonality between the bound and continuum states of H_2^+. Our procedure differs from other approaches in which dynamical information is extracted by projecting the propagated wavepacket directly onto unperturbed final states. For example, in the work of Colgan, Pindzola and Robicheaux [5] to which we will be comparing, the total ionization probability is computed as $1 - P_b$, where P_b is the probability of bound-state excitation, computed by projection onto the complete set of bound states of H_2^+ obtained by diagonalizing H_0. This procedure does not

TABLE I: The selection rule on quantum numbers l and m in Eq. (16), depends on the possible transitions between the states with different symmetries.

	l values	m values	polarization[a]
One-photon ionization			
$\Sigma_g \to \Sigma_u$	odd	0	$\parallel$
$\Sigma_g \to \Pi_u$	odd	± 1	$\perp$
$\Pi_u \to \Sigma_g, \Delta_g$	even	0, ± 2	$\perp$
Two-photon ionization			
$\Sigma_g \to \Sigma_u \to \Sigma_g$	even	0	$\parallel$
$\Sigma_g \to \Pi_u \to \Sigma_g, \Delta_g$	even	0, ± 2	$\perp$

[a]linear polarization of the field corresponding to the internuclear molecular axis, $\parallel$ means parallel, $\perp$ means perpendicular.

directly distinguish between various n-photon processes, so additional assumptions are then required to compute specific n-photon total cross sections, and angular distributions are not available.

C. One and two-photon ionization cross sections

Assuming the field intensities are such that we are in the perturbative limit, we can use the extracted ionization amplitudes to calculate cross sections, corresponding to different photon absorption processes, for any frequency within the band width of a pulse ($\Delta\omega = 4\pi/T$ for a sine-squared time envelope . For single ionization, the differential and total photoionization cross sections are given by [3]

$$\begin{aligned} \frac{d\sigma_1}{d\Omega} &= \frac{4\pi^2 kc}{\omega_{ik}} \frac{|C(\mathbf{k})|^2}{|A_0|^2 \left|\widetilde{F}^{(1)}(\omega, \omega_{ik}, T)\right|^2} \\ \sigma_1 &= \frac{4\pi^2 kc}{\omega_{ik}} \frac{\sum\limits_{l_0,m} \left|c_{l_0,m}(k)\right|^2}{|A_0|^2 \left|\widetilde{F}^{(1)}(\omega, \omega_{ik}, T)\right|^2} \end{aligned} \tag{18}$$

where ω_{ik} is the energy difference between the final continuum state and the initial ground state, $\omega_{ik} = E_k - E_i$, and $\widetilde{F}^{(1)}$ is the shape function for single photon ionization. For a sine-squared pulse its squared modulus is given analytically by [3]

$$|\widetilde{F}^{(1)}(\omega, \omega_{ki}, T)|^2 = \frac{4\pi^4 \sin^2((\omega - \omega_{ki})T/2)}{(T^2(\omega - \omega_{ki})^2 - 4\pi^2)^2(\omega - \omega_{ki})^2}, \tag{19}$$

We note that the factorization of the time dependence from the amplitude for single photon absorption in lowest order perturbation theory ensures that Eq. (18) is strictly independent of the pulse length T.

For two-photon ionization, we present results in the form of differential and total generalized cross sections (in units of $\mathrm{cm}^4\mathrm{W}^{-1}$) [3, 6]:

$$\begin{aligned} \frac{dQ^{(2)}/I}{d\Omega} &= \frac{2\pi^2 kc^3}{\bar{\omega}_{ik}^3 I_0} \frac{|C(\mathbf{k})|^2}{|A_0|^4 \left|\widetilde{F}^{(2)}(\omega, \bar{\omega}_{ik}, T)\right|^2} \\ Q^{(2)}/I &= \frac{2\pi^2 kc^3}{\bar{\omega}_{ik}^3 I_0} \frac{\sum\limits_{l_0,m} \left|c_{l_0,m}(k)\right|^2}{|A_0|^4 \left|\widetilde{F}^{(2)}(\omega, \bar{\omega}_{ik}, T)\right|^2}, \end{aligned} \tag{20}$$

where I_0 is the atomic unit of intensity (1a.u. = 7.0189 $\times$ 10^{16} W/cm^2), $\bar{\omega}_{ik} = (E_k - E_i)/2$ and $\widetilde{F}^{(2)}$ is the shape function for two-photon absorption, which we approximate as [3]

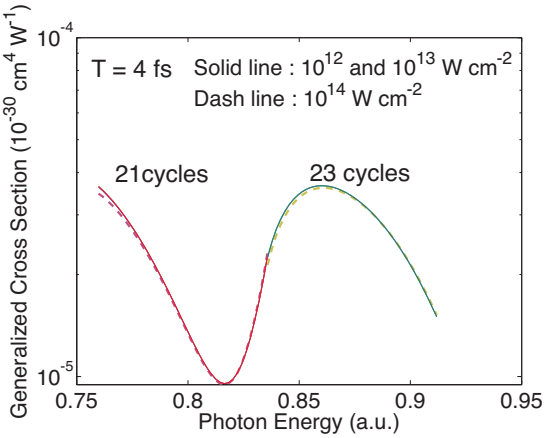

FIG. 1: (Color online) Two-photon generalized cross sections for H_2^+ with parallel photon polarization. Calculations carried out with pulse intensities 10^{12}, 10^{13} and 10^{14} W cm^{-2}. Results are extracted from calculations using 4 fs pulses with bandwidth of 21 and 23 cycles, respectively. Photon energies in atomic units. 1 a.u. = 27.211 eV.

$$\widetilde{F}^{(2)}(\omega, \omega_{ki}, T) = \frac{6e^{-iT(2(\omega-\bar{\omega}_{ki}))}\left(-1 + e^{iT(2(\omega-\bar{\omega}_{ki}))}\right)\pi^4}{(2(\omega - \bar{\omega}_{ki}))\left(T^4(2(\omega - \bar{\omega}_{ki}))^4 - 20\pi^2T^2(2(\omega - \bar{\omega}_{ki}))^2 + 64\pi^4\right)}. \tag{21}$$

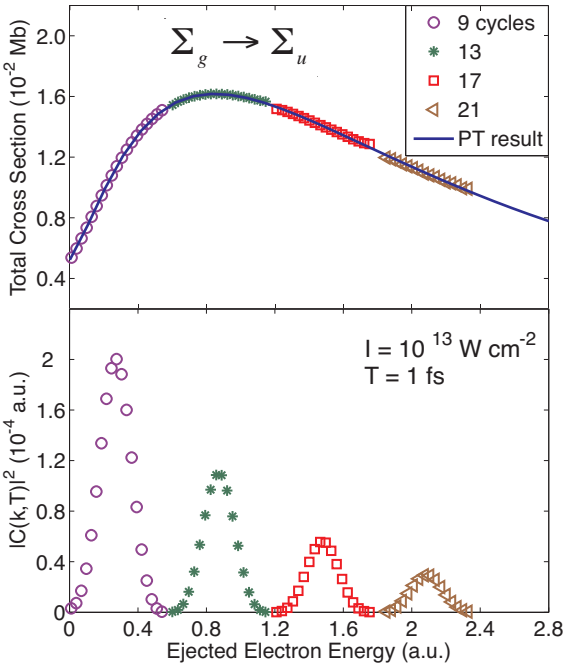

FIG. 2: (Color online) Top panel : H_2^+ one photon ionization cross section from Σ_g ground state to Σ_u continuum states extracted from pulses with varying central frequencies. Linear photon polarization parallel to the molecular axis. Solid line: time-independent perturbation theory result. Lower panel : the squared amplitudes extracted from 1 fs pulses with 13, 17 and 21 cycles, from which the top panel is calculated. Cross section in units of megabarns. 1 Mb=10^{-18}cm^2.

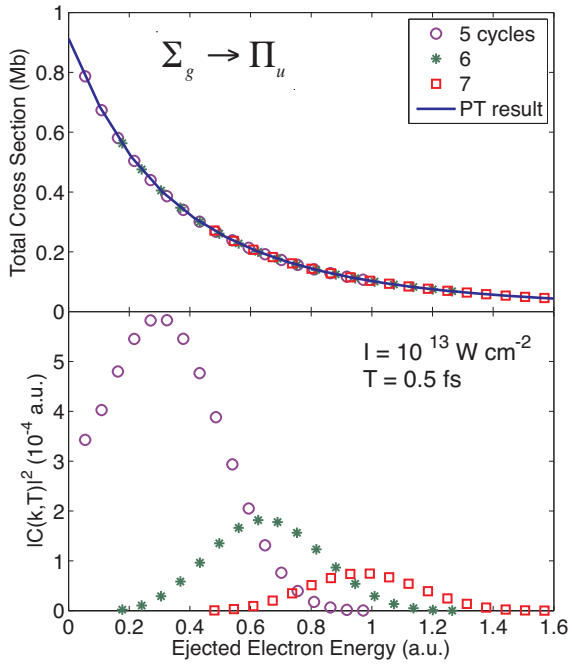

FIG. 3: (Color online)As inFig. 2, but with photon polarization perpendicular to the molecular axis, pulse duration T=0.5 fs with 5, 6 and 7 cycles.

We must emphasize that, in contrast to the one-photon case, the factorability of the transition probability in the two-photon case is only approximate and breaks down when the pulse width is very short or when the photon frequency is close to being in resonance with a discrete intermediate state, in which case long propagation times may be required to resolve the energy dependence of the cross section near narrow resonance features.

III. RESULTS

The time-dependent Schrödinger equation was solved by propagating an initial wavepacket with pulse lengths of 1, 4 and 8 fs on real-valued grids of length (ξ_{max}) 150, 270 and 500, respectively. The grids were subdivided into finite elements; the first element runs from $\xi = 0$ to $\xi = 1$, while subsequent elements are of length 8.25 to 10.0. 15th order DVR was used in each element. The wavepacket at the end of the pulse was used as the source term in the driven equation for the scattered wave which was solved under ECS. For this purpose, the original real grid was augmented with an additional segment of length 30, rotated into the complex plane by 20 degrees. We used 15th-order DVR Over the range of photon energies considered here, we found that convergence could be achieved with $l_{max} = 5$ in prolate spheroidal coordinates and that the numerical accuracy required with the chosen density of grid points could be achieved with a time step 0.02 a.u.

We have restricted our calculations to field strengths where perturbation theory can be applied and, therefore, a cross section defined. In this way, we can check the accuracy of our results by comparing with existing calculations, where available. In Fig. 1, we show the two-photon generalized cross sections for parallel polarization obtained for intensities of 10^{12}, 10^{13} and 10^{14} W cm^{-2}. At $I = 10^{14}$ W cm^{-2} the result shows a weak dependence on intensity. We therefore chose $I = 10^{13}$ W cm^{-2} for the reported calculations, which is high enough to produce relatively large ionization rates, while still keeping the one and two-photon ionization results within the perturbative regime.

For the results we are presenting, the calculations were all carried out the the equilibrium internuclear separation of H_2^+, $R = 2.0$ bohr.

A. Single photon ionization

The total cross sections for one photon ionization of H_2^+ in its ground electronic state, for photon polarization parallel and perpendicular to the molecular axis, are shown in the top panels of Figs. 2 and 3, respectively. Fig. 4

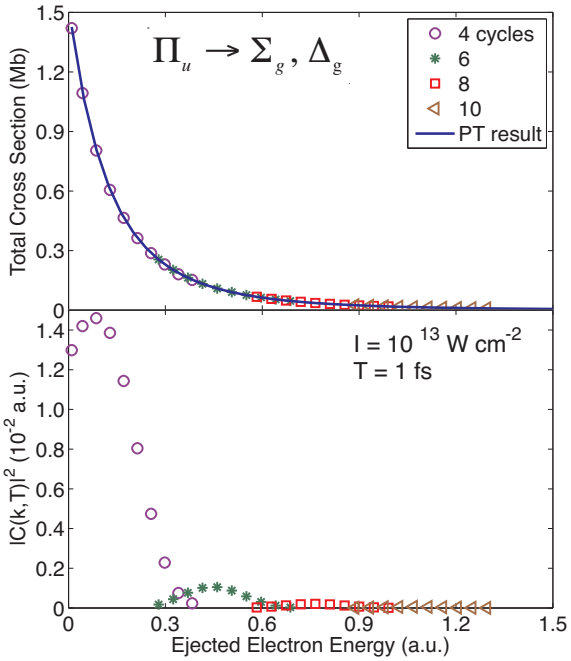

FIG. 4: (Color online) As in Fig. 3, except that H_2^+ initial state is the first eigenstate of Π_u symmetry, pulse duration T =0.5 fs with 4, 6, 8 and 10 cycles.

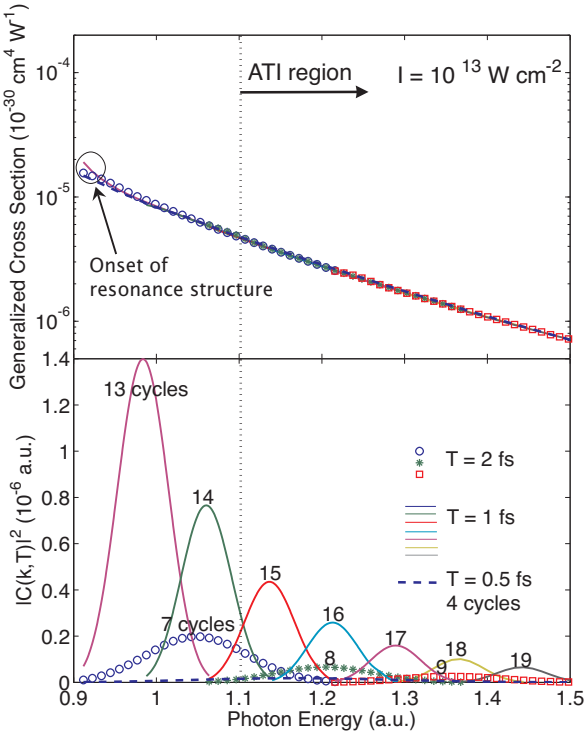

FIG. 5: (Color online) Top panel: two-photon generalized cross sections in the ATI region calculated with pulses of 0.5, 1 and 2 fs as functions of photon energy. Field linear polarization parallel to molecular axsis. Lower panel: Squared amplitudes in atomic units, from which the cross sections in the top panel were calculated.

shows results for the case of ionization starting from the first Π_u state of H_2^+ for the case of perpendicular polarization. These cross sections were extracted from calculations using different central frequencies of the field, i.e. different numbers of optical cycles, as indicated in the figures. The lower panels of these figures show the corresponding squared amplitudes from which the cross sections were extracted. The time-dependent results are seen to be in perfect agreement with the results obtained using time-independent perturbation theory, confirming the fact that there are essentially no approximations involved in the extraction procedure, even for the sort pulse lengths employed in these calculations [3].

B. Two-photon ionization

We turn next to an investigation of two-photon ionization with pulses of varying length. Fig. 5 shows the two-photon generalized total cross section in the above-threshold ionization (ATI) region from the Σ_g ground state to Σ_g continuum states (parallel polarization). For photon energies above the ATI threshold (1.1 a.u.), the extracted cross sections decrease monotonically and are relatively insensitive to changes in pulse length from T = 0.5 fs to 2 fs. However, for photon energies near 0.9 a.u., the effect of intermediate state resonances begins to appear with longer pulse lengths.

The dependence of the extracted two-photon cross sections on pulse length is further examined in Figs. 6 and 7, which show results obtained using relatively long pulses of 4 fs and 8 fs, respectively. The effect of intermediate state resonances is evident in these figures; their structure becomes better resolved as the pulse length is increased. In the lower panels of those figures we can see the resonant behavior in the excitation amplitudes, $C(k,T)$, for example near the curve labeled "23 cycles" in 6 . Table II lists the first few intermediate bound states in both Σ_u and Π_u symmetries. Note that the lowest Σ_u state of H_2^+ lies below the two-photon ionization threshold and that the first resonance peak arises from the $3p\sigma_u$ state. We note that, away from resonances, our results are in excellent agreement with the time-independent Floquet calculations of Plummer and McCann [7], as well the time-independent calculations of Baik *et al.* [8], Apalategui *et al.* [9] and Palacios *et al.* [10](not shown). Also plotted are the time-dependent results of Colgan *et al.* [5]. Because of the relatively short propagation times employed in those calculations (15-20 field cycles), no resonance structure was resolved and some intensity dependence is evident in their derived cross sections as well.

Figure 8 shows calculations for the case of photon polarization perpendicular to the molecular axis. Pulse durations extend up to 4 fs. In this case, we are able to observe resonance peaks starting from the first interme-

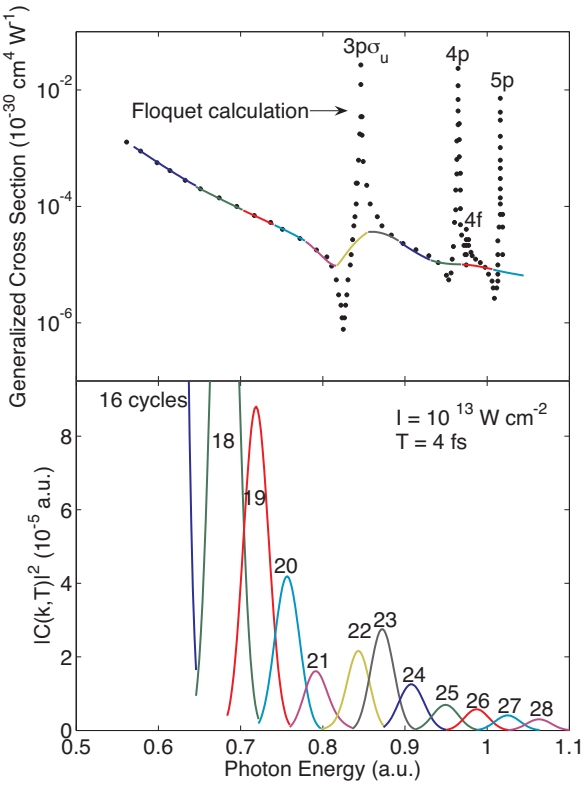

FIG. 6: (Color online) As in Fig. 5, with a T= 4 fs pulse. The positions of resonance peaks from different intermediate states of Σ_u symmetry are labeled on the plot. Dots: Floquet calculation results of Plummer and McCann [7]. Squares and triangles: results of Colgan *et al.* [5] at intensities of 10^{13} and 10^{14} W cm^{-2}, respectively.

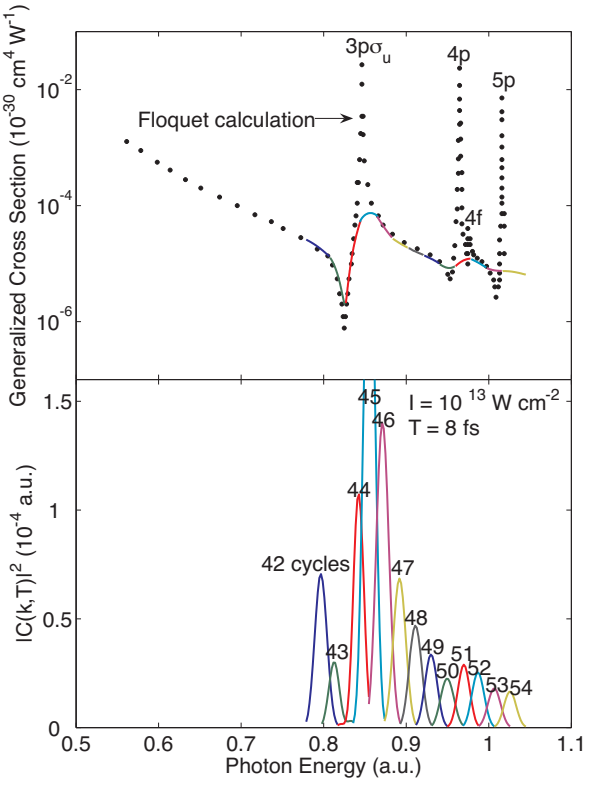

FIG. 7: (Color online) As in Fig. 6, with a T = 8 fs pulse.

diate state in Π_u symmetry. Since the first resonance peak at photon energy 0.68 a.u. is relatively close to the two-photon ionization threshold (0.55 a.u.), there is a relatively strong dependence near threshold in the extracted cross section on the pulse length used. Our results for this case are again found to be converging, as the pulse length is increased, to the the results of time-independent lowest order perturbation theory, as seen by comparison with the results of Apalategui *et al.* [9]. We have also plotted the time-dependent results of Colgan *et al.* [5], which evidently show a stronger dependence on field intensity than was the case for parallel photon polarization.

Finally, we present results for molecular frame photoelectron angular distributions for two -photon ionization. Figure 9 shows results for both parallel and perpendicular photon polarization at three different photon energies, 0.68, 0.86 and 1.12 a.u. For the parallel case, the three photon energies fall below the 3pσ_u resonance, near that resonance and in the ATI region, respectively. The displayed results (solid curves) were obtained from calculations with a 4 fs pulse. Not surprisingly (see Fig. 7), calculations with an 8 fs pulse change the magnitude of

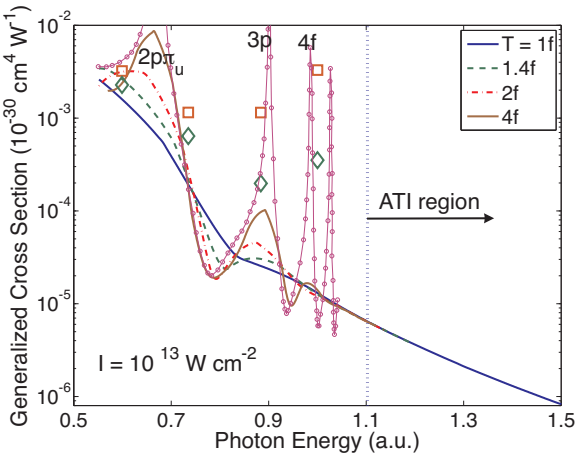

FIG. 8: (Color online)Two-photon generalized cross sections for the case of perpendicular photon polarization calculated with pulses of 0.5, 1 and 2 fs. as functions of photon energy. The positions of resonance peaks from different intermediate states of Π_u symmetry are labeled on the plot. Solid curve with dots: time-independent results of Apalategui *et al.* [9]. Squares and diamonds: results of Colgan *et al.* [5] at intensities of 1.76×10^{13} and 1.76×10^{14} W cm^{-2}, respectively.

TABLE II: H_2^+ excited-state energies, and corresponding excitation energies from the ground state ($E_0 = -1.10263$ a.u.), in Σ_u and Π_u symmetries at internuclear distance $R = 2$ a.u. Two-photon ionization starts at photon energy 0.55132 a.u.

	E_n (a.u.)	$E_n - E_0$ (a.u.)
Σ_u states		
$2p\sigma_u$	-0.667534	0.43510
$3p\sigma_u$	-0.255413	0.84722
$4p\sigma_u$	-0.177681	0.92495
$4f\sigma_u$	-0.126644	0.97599
Π_u states		
$2p\pi_u$	-0.428772	0.67386
$3p\pi_u$	-0.200865	0.90177
$4f\pi_u$	-0.126199	0.97643

the results at 0.86 a.u. photon energy, but not the results at the other two energies. The shapes of the distributions are evidently insensitive to changing the pulse length. The cylindrically symmetric distributions, which contain only Σ_g final state contributions for the case of parallel photon polarization, are strongly peaked along the molecular axis. The coherent combination of significant s- and d-wave final state contributions results in an almost complete extinction of probability for photoejection at 90 degrees to the molecular axis. Moreover, the shape of the distributions show surprisingly little dependence on photon energy and differ from the time-dependent results of Selsto *et al.* [11].

Figure 9 also shows results for the case of photon polarization perpendicular to the molecular axis at the same three energies. In this case, the photoelectron angular distributions are not cylindrically symmetric, so we show results in the plane defined by the polarization vector and the molecular axis (middle column), and perpendicular to that plane (right column). One can see (from Fig. 8) that the chosen photon energies now sample the $2p\pi_u$ resonance, $3p\pi_u$ resonance and ATI regions, respectively. In this case, there are final state contributions from both Σ_g and Δ_g symmetries, the latter evidently making the dominant contribution and breaking the cylindrical symmetry of the angular distributions. Unfortunately, there are, to our knowledge, no other results available for comparison in this case.

IV. DISCUSSION

We have shown that a finite-element/DVR approach can be specially tailored for application to diatomic targets by using prolate spheroidal coordinates and can provide a very accurate approach for solving the time-dependent Schrödinger equation. We have demonstrated this idea with illustrative calculations of one- and two-photon ionization of H_2^+. By working with field intensities where perturbation theory is valid, we have extracted total cross sections, for photon polarization parallel and perpendicular to the molecular axis, that can be directly compared with the results of time-independent calculations employing lowest order perturbation theory. We have also presented results for molecular-frame photoelectron angular distributions for two-photon ionization. While these calculations have all be carried out within the fixed nuclei approximation, a primary motivation for this work have been the development of an approach that is accurate and efficient enough to be extended to studies which explicitly consider nuclear motion beyond the Born-Oppenheimer approximation. Such investigations will be the subject of future work.

Acknowledgments

This work was performed under the auspices of the US Department of Energy by the University of California Lawrence Berkeley National Laboratory under Contract DE-AC02-05CH11231 and was supported by the U.S. DOE Office of Basic Energy Sciences, Division of Chemical Sciences. CWM acknowledges support from the NSF (PHY-0604628).

[1] L. Tao, C. W. McCurdy, and T. N. Rescigno, Phys. Rev. A **79**, 012719 (2009).
[2] S. Balay, K. Buschelman, V. Eijkhout, W. D. Gropp, D. Kaushik, M. G. Knepley, L. C. McInnes, B. F. Smith, and H. Zhang, Tech. Rep. ANL-95/11 - Revision 2.1.5, Argonne National Laboratory (2004).
[3] A. Palacios, C. W. McCurdy, and T. N. Rescigno, Phys. Rev. A **76**, 043420 (2007).
[4] A. Palacios, T. N. Rescigno, and C. W. McCurdy, Phys. Rev. A **77**, 032716 (2008).
[5] J. Colgan, M. S. Pindzola, and F. Robicheaux, Phys. Rev. A **68**, 063413 (2003).
[6] E. Karule, J. Phys. B **11**, 441 (1978).
[7] M. Plummer and J. F. McCann, J. Phys. B **28**, 4073 (1995).
[8] M.-G. Baik, M. Pont, and R. Shakeshaft, Phys. Rev. A. **54**, 1570 (1996).
[9] A. Apalategui, A. Saenz, and P. Lambropoulos, J. Phys. B **33**, 2791 (2000).
[10] A. Palacios, S. Barmaki, H. Bachau, and F. Martín, Phys. Rev. A **71**, 063405 (2005).
[11] S. Selsto, A. Palacios, J. Fernández, and F. Martín, Phys. Rev. A **75**, 033419 (2007); we have been informed by these authors that a phase error was made in the calculation of their angular distribitions.

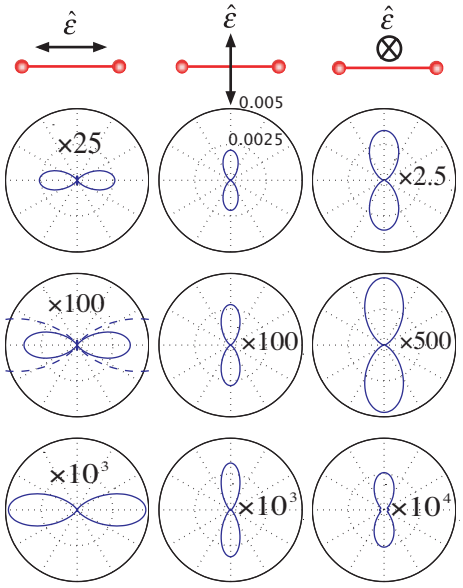

FIG. 9: (Color online)Differential two-photon generalized cross sections, in units of 10^{-30} cm^4/ W/ sr, extracted from calculations with a 4 fs pulse (Dashed curve in left center panel is for an 8 fs pulse). Left column: angular distributions with photon polarization parallel to molecular axis. Center column: angular distributions in the plane defined by photon polarization vector and molecular axis, with polarization vector perpendicular to molecule. Right column: angular distribution in plane perpendicular to that used in center column. Photon energies, row-wise top to bottom, are 0.68, 0.86 and 1.12 a.u.